Title: A modular platform to display multiple hemagglutinin subtypes on a single immunogen

Authors: Dana Thornlow Lamson[1,2], Faez Amokrane Nait Mohamed[1], Mya Vu[1], Daniel P. Maurer[1,2], Larance Ronsard[1], Daniel Lingwood[1], Aaron G. Schmidt[1,2*]

Affiliations: [1]Ragon Institute of Mass General, MIT, and Harvard, Cambridge, MA, 02139, USA

[2]Department of Microbiology, Harvard Medical School, Boston, MA 02115, USA

Key words: influenza, immunogen design, nanoparticle, vaccine, hemagglutinin, protein engineering

Correspondence:
Aaron G. Schmidt
Tel: 857-268-7118
E-mail: aschmidt@crystal.harvard.edu

ABSTRACT

Next-generation influenza vaccines aim to elicit cross-reactive humoral responses to multiple influenza subtypes. Such increased breadth would not only improve seasonal vaccines but may afford 'universal' protection against influenza subtypes including those with pandemic potential. Here, we describe a "beads-on-a-string" (BOAS) immunogen, that tandemly links up to eight distinct hemagglutinin (HA) head domains from circulating and non-circulating influenzas. These BOAS are immunogenic in the murine model and elicit comparable serum responses to each individual component. Notably, we also find that BOAS elicit cross-reactive responses to influenza subtypes not included in the immunizing immunogen. Furthermore, BOAS conjugation to protein-based ferritin nanoparticles does not significantly augment serum responses suggesting that our BOAS platform is sufficient for eliciting cross-reactive responses without off-target effects induced by the nanoparticle scaffold. Finally, vaccination with a mixture of the same HA head domains is not sufficient to elicit the same neutralization profile as the BOAS immunogens or nanoparticles. This mix-and-match immunogen design strategy is a robust platform for eliciting responses to multiple influenza subtypes via a single immunogen, and a potential platform for other viral glycoproteins.

INTRODUCTION

Influenza viruses, despite continuous surveillance and annual vaccination, are a significant public health problem resulting in ~500,000 deaths per year[1]. This is largely a consequence of viral evolution and antigenic drift as it circulates seasonally within humans and ultimately impacts vaccine effectiveness. Additionally, the chance for spillover events from animal reservoirs (*e.g.,* avian, swine) is increasing as population and connectivity also increase. To combat this, global surveillance is necessary to inform re-formulation of influenza vaccines to match circulating strains. However, long lead times for vaccine preparation in eggs and mutations acquired during that process[2] can lead to vaccine mismatch and subsequent ineffectiveness. The SARS-CoV-2 pandemic has additionally underscored the need for pandemic preparedness as humans increasingly come into contact with animal reservoirs. Indeed, several avian influenzas, such as H5N1, H7N9 and H9N2, are currently being monitored for their pandemic potential. Thus, there is an urgent need to develop so-called "universal" influenza vaccines that provide protection against both currently circulating (*e.g.,* H1N1s, H3N2s, and Bs) and potentially pandemic viruses.

Several approaches have been taken to improve upon current influenza vaccines, largely focused on the influenza surface glycoprotein, hemagglutinin (HA). A major goal of immunogen design efforts is to elicit antibodies toward conserved epitopes on HA, including the receptor binding site (RBS)[3–9], trimer interface[10–14], and stem[15–20]; antibodies targeting such epitopes are often broadly protective. Indeed, RBS-directed antibodies often are potently neutralizing, as they directly inhibit HA engagement with host cell sialic acid, while TI- and stem-directed antibodies generally protect via Fc-dependent mechanisms (*e.g.,* ADCC, ADCP). Several rational immunogen design approaches[21] such as epitope removal[22,23], domain chimeras[24], computational sequence optimization (COBRAs)[25–29], epitope resurfacing[30] and hyperglycosylation[14,31,32] attempt to focus to these epitopes.

An additional strategy to enrich for cross-reactive antibodies includes increasing antigen valency by displaying multiple antigens on a scaffold, such as a nanoparticle[33–35]. Such multivalency is thought to enhance immunogenicity and antigenicity by spacing antigens near one another in order to effectively cross-link B cell receptors (BCRs)[36]. Ferritin, which can display 24 antigens at its 8 three-fold axes, has been used for influenza, Epstein-Barr virus, coronavirus, and HIV

glycoproteins[37–43]. For influenza, following immunization with a mixture of homotypic full-length seasonal H1, H3, and influenza B HA trimers displayed on ferritin nanoparticles, mice elicited responses with enhanced potency and breadth relative to the trivalent inactivated influenza vaccine (TIV) standard[38]. Based on this success, they then designed "mosaic" ferritin nanoparticles that displayed up to eight antigenically distinct H1 subtype HA receptor binding domains (RBDs) on a single particle, which outperformed admixtures of homotypic nanoparticles and elicited cross-reactive H1 broadly neutralizing antibodies[41]. Further iterations of nanoparticle immunogens have co-displayed multiple full-length HA antigens on virus-like particles (VLPs)[44] and *de novo* designed particles[45], and the latter is currently in clinical trials[45,46,47].

An alternative approach for multivalent display involves tandemly linking antigens into a single polypeptide. This method may alleviate manufacturing challenges related to preparing multiple individual components for mosaic nanoparticles while still increasing size and valency of antigens. For example, using domain III from the dengue envelope surface glycoprotein, a bivalent[46] or quadrivalent[47] tandemly linked immunogen elicited neutralizing antibody responses to all four dengue serotypes and provided protection upon challenge. An analogous approach tandemly linked four different coronavirus RBDs into a single immunogen[48]. These "quartets" elicited responses to each individual components similar to a "mosaic-4" nanoparticle that displayed monomeric RBDs on the surface of a virus like particle (VLP) nanoparticle[49,50]; these approaches were then combined and quartets displaying four or eight unique RBDs were multivalently displayed on VLP nanoparticles. This combinatorial approach augmented both neutralization titers and cross-reactive responses.

Here, we tandemly linked multiple HA subtypes into a single immunogen via short, flexible linkers in a "plug and play" platform we call "beads-on-a-string" or BOAS. These recombinantly produced, protein-based immunogens have between three and eight unique HA heads including circulating and non-circulating A and B influenzas. Mice immunized with either 3, 4, 5, 6, 7, or 8mer BOAS elicited responses to matched and mismatched HA components and could neutralize subsequent replication-restricted reporter (R3) viruses[51]. To further enhance valency, we generated two 4mer BOAS that included 8 different HA heads, conjugated both to ferritin nanoparticles using SpyTag-SpyCatcher[52,53], and showed that the serum responses elicited similar responses to the

105 8mer. Additionally, we showed that a mixture of the same HA head components was not sufficient
106 to recapitulate the neutralizing responses elicited by the BOAS or BOAS NP. Collectively, these
107 BOAS immunogens could serve as a means to elicit responses to multiple HA subtypes as a single
108 immunogen and represents a general approach for multivalent display of other viral antigens.
109
110
111 **RESULTS**
112
113 **Design and characterization of beads-on-a-string (BOAS)**
114 Monomeric hemagglutinin (HA) heads representing antigenically distinct subtypes were tandemly
115 linked together as a single linear construct, separated by a short, flexible glycine-serine-serine
116 (GSS) linker, which we termed beads-on-a-string (BOAS) immunogens. Eight unique HA
117 subtypes spanning group 1 and 2 influenza A viruses, as well as an influenza B virus, from
118 seasonal, circulating, and non-circulating influenzas were selected to understand the permissibility
119 of the platform to express different HAs (**Figure 1A**). We found that monomeric HA head domains
120 varied in expression levels depending on the boundaries selected: H1, H5, and H7 HA monomers
121 spanned residues 57-261 (H3 numbering), whereas H2, H3, H4, H9, and B HA monomers spanned
122 residues 37-316 (H3 numbering) (**Figure 1B**). We then asked whether we could tandemly link
123 multiple HA heads together as a single construct. Using linkers with either two, three, or four GSS
124 repeats, we tandemly linked representative H1, H3, and B HAs (**Supplemental Figure 1A**)
125 together for recombinant expression in mammalian cells. Each construct, regardless of linker
126 length expressed to similar levels (**Supplemental Figure 1B**) and each individual HA component
127 could be detected with a conformation specific and subtype specific monoclonal antibody (mAb)
128 (**Supplemental Figure 1C**). We next assessed whether the order of the HA heads adversely
129 affected expression or accessibility to the conformation-specific mAb. Using H5, H7, and H9 HA
130 heads we created two constructs 1) H5-H9-H7 and 2) H9-H5-H7 each with a four GSS linker.
131 Each construct had comparable levels of expression and reactivity to the respective mAbs
132 (**Supplemental Figure 2**).
133
134 Based on these initial data, we next designed six constructs with three to eight individual HA head
135 components from representative H1, H2, H3, H4, H5, H7, H9, and B influenzas; to maximize

136 spacing between each HA component we used the 4x GSS linker. Each BOAS was cloned into a
137 single polypeptide chain with a protease-cleavable C-terminal purification tag (**Figure 1C**). We
138 synthesized six different BOAS, and define each construct as 3mer, 4mer, etc., referencing the
139 number of HA components (**Figure 1D**). Each BOAS construct could be purified to homogeneity
140 as assayed by SDS-PAGE after immobilized metal affinity chromatography (**Figure 2A**) and
141 correspond to the expected molecular weight following proteolytic cleavage of native glycans with
142 PNGase-F (**Figure 2B**). After size-exclusion chromatography (SEC), the non-PNGase-treated
143 BOAS were monodispersed (**Figure 2C**). Following SEC, affinity tags were removed with HRV-
144 3C protease; cleaved tags, uncleaved BOAS, and His-tagged enzyme were removed using cobalt
145 affinity resin and snap frozen in liquid nitrogen before immunizations. BOAS maintained
146 monodispersity upon thawing, though over time, degradation was observed following longer term
147 (>1 week) storage at 4C (**Supplemental Figure 3)**. This degradation became more significant as
148 BOAS increased in length (**Supplemental Figure 3)**.
149
150 We then analyzed the BOAS using negative stain electron microscopy (NS-EM). Individual HAs
151 were readily discernable and equal to the number of components in the respective BOAS (**Figure**
152 **2D and 2E**); we observed that the 3mer could adopt both extended and collapsed, triangular-like
153 conformations (**Figure 2D**), whereas longer BOAS, such as the 8mer, adopted a rosette-like
154 conformation (**Figure 2E**). This is likely a consequence of the flexible GSS linker separating the
155 individual HA head components as well as the addition of significantly more HA head components
156 to the construct.
157
158 To assess conformational integrity and ensure that each HA present was properly folded, we
159 assembled a panel of conformation- and subtype-specific mAbs to assay each individual
160 component. This included mAb S5V2-29[12] a broadly-reactive TI-directed positive control
161 antibody and mAbs 5J8[4,6], 2G1[5], K03.12[54], P2-D9[55] (**Supplemental Figure 4**), H5.3[56], H7.167[57],
162 and H1209[58] which are specific to H1, H2, H3, H5, H5, H7 and B subtypes, respectively; an H9
163 conformation-specific mAb was not available. Each individual HA component was detected using
164 subtype-specific mAb in ELISA, and overall affinity for each component was comparable
165 regardless of BOAS length (**Figure 2F**). Collectively, these data support a plug-and-play platform
166 that can readily exchange HA components while retaining conformational integrity.

167

168 **Immunogenicity of BOAS**

169 To determine immunogenicity of each BOAS immunogen, we performed a prime-boost-boost
170 vaccination regimen in C5BL/6 mice at two-week intervals with 20µg of immunogen and
171 adjuvanted with Sigma Adjuvant (**Figure 3A**). We compared these BOAS to a control group
172 immunized with a mixture of the eight HA heads present in the 8mer. We then tested serum
173 reactivity to both BOAS immunogen as well as individual full-length HA trimers of each
174 component. Serum titers against the immunogen were detectable after a single prime, and
175 increased following a boost, and stayed relatively level until day 42 (**Figure 3B**). Serum responses
176 varied for differing BOAS lengths, with the 4mer and 5mer BOAS being the most immunogenic
177 (**Figure 3C**). Each of the BOAS, regardless of its length, elicited binding titers to all matched full-
178 length HAs representing individual components (**Figure 3D**). For example, the 6mer, which
179 contains heads of H1, H2, H3, H4, H5, and H7, elicited reactivity to full length matched HAs.
180 Interestingly, some BOAS elicited cross-reactivity to mis-matched components not present in the
181 immunogen. For example, the 3mer, which contained H1, H2, and H3 HA heads, elicited
182 detectable titers to H4 and H5 HAs (**Figure 3D**). Additionally, all groups elicited binding titers to
183 mismatched historical H3 and H1 HAs (Figure 3D). When comparing the 8mer and mix groups,
184 the 8mer tended to elicit stronger binding titers to matched and mismatched components than an
185 equal molar mixture of the same components (**Figure 3E**). Similar binding trends were also
186 observed with d28 serum, though the difference between the 8mer and mix groups was more
187 pronounced at d28 (**Supplemental Figure 5**).

188

189 **Cross-reactivity of immune responses**

190 To understand potential cross-reactivity observed in the serum analyses, across we used a Consurf-
191 like[59,60] method to assess sequence conservation across the eight HA components in the BOAS.
192 Each component of the BOAS was aligned structurally to the H2 head domain and scored at each
193 position for their amino acid conservation at each position on a scale of 1 to 9. These were then
194 pseudo-colored on the structure to visualize conserved and variable epitopes on the head domain
195 surface (**Figure 4A**). We observed regions of both significant variability as well as conservation,
196 notably the TI epitope, as well as the core sialic acid interacting residues in the receptor binding
197 site (RBS), the latter which remained nearly 100% conserved in all BOAS (**Figure 4A**). This was

198 quantitated by taking the average amino acid (AA) conservation score across both the RBS and TI
199 epitopes as well as the entire sequence, and we see that these epitopes retain higher conservation
200 relative to the overall sequence as BOAS length increases. We then determined approximate
201 degrees of focusing to the TI and RBS via a serum competition ELISA using mAbs. All the BOAS
202 maintained, approximately, between 15-35% focusing to the TI epitope, whereas focusing the RBS
203 was more variable (**Figure 4C**). Both RBS focusing (**Figure 4D**) and TI focusing (**Figure 4E**)
204 trended similarly with homology scores for each epitope, indicating epitope conservation may be
205 influencing immune focusing to particular epitopes.
206
207 **Design of BOAS-conjugated nanoparticles**
208 To further increase avidity affects as well as potential immunogenicity, we split our 8mer BOAS
209 into two 4mer BOAS and attached both in an equal molar ratio to *H. pylori* ferritin nanoparticles
210 (NPs) using SpyTag-SpyCatcher[52], herein referred to as BOAS-NPs (**Figure 5A**). The two 4mer
211 BOAS efficiently conjugated to nanoparticles as determined by SEC and SDS-PAGE
212 (**Supplemental Figure 6**), Further biophysical characterization using dynamic light scattering
213 (DLS) showed a shift of from 9.8 ± 1.1 nm to 21.3 ± 2.0 nm and NS-EM showed spherical particles
214 with projections. (**Figure 5D and 5E**). We verified the presence and structural integrity of each
215 BOAS component on the nanoparticles using an ELISA with the same panel of conformation and
216 subtype-specific mAbs, (**Figure 5E**).
217
218 **Immunogenicity of BOAS-conjugated nanoparticles**
219 We next immunized mice with BOAS-NP and a SpyCatcher NP control to assess immunogenicity.
220 Mice were immunized with an equal amount of NP relative to the BOAS (20µg), in an equivalent
221 homologous prime-boost-boost regimen (**Figure 6A**). The BOAS-NP was significantly more
222 immunogenic than the SpyCatcher NP control, eliciting titers approximately an order of magnitude
223 greater by d42 (**Figure 6B**). The BOAS NP, however, elicited significantly reduced titers to the
224 SpyCatcher NP scaffold relative to the control (**Figure 6C**). When each group was evaluated for
225 titers against both the BOAS components, the SpyCatcher nanoparticle scaffold, or BOAS-NP
226 (**Figure 6D,E**), the BOAS-NP elicited equivalent titers to each set of BOAS, and greater titers to
227 the decorated nanoparticle relative to the ferritin scaffold (**Figure 6E**). When we examined titers
228 to individual HA components, we observed detectable titers over baseline to all eight HAs present

229 on the BOAS-NPs (**Figure 6F**). When compared to the immunogenicity of the 3mer to 8mer
230 BOAS immunogens, the BOAS-NP showed comparable titers to each component relative to
231 BOAS that contained a given component (**Figure 6G**).
232
233 **Neutralization of influenza viruses by BOAS-elicited sera**
234 We next determined serum neutralization titers to matched and mis-matched influenza viruses
235 based on the BOAS components (**Figure 7**). We tested serum from mice immunized with all
236 BOAS against H1/Michigan/2015 H1N1 and H3/Kansas/2017 H3N2 viruses, whose HA was
237 present in all the BOAS. These showed varying neutralization titers to both viruses, with all
238 matched BOAS neutralizing virus except for the 7mer and H1N1 virus. Additionally, we tested
239 serum against H5/Vietnam/2004 H5N1 and H7/Shanghai/2013 H7N9 viruses. Neutralization of
240 H5N1 virus was variable, though individual mice from 4mer, 5mer, 6mer, 7mer, 8mer, and BOAS
241 NP groups were able to strongly neutralize this virus. Weak neutralization titers were detected for
242 6mer, 7mer, and 8mer BOAS. This neutralization was only slightly above the high background
243 neutralization of the negative control NP serum. Serum from the BOAS-conjugated nanoparticle
244 group elicited similar neutralization titers relative to the BOAS alone. In most cases, neutralization
245 titers elicited from the BOAS and BOAS NP cohorts were greater than that from the mix cohort.
246 The scaffold control serum did not neutralize any viruses tested.
247
248 **DISCUSSION**
249 Here we engineered "beads-on-a-string" (BOAS) that included tandemly linked, antigenically
250 distinct HA heads as a single construct. This platform allows a mixing-and-matching of up to eight
251 distinct HA heads from both influenza A and B viruses. Furthermore, we showed that the order
252 and number of HA heads can vary without losing reactivity to conformation-specific mAbs *in*
253 *vitro*, highlighting the flexibility of this platform. Mice immunized with BOAS had comparable
254 serum reactivity to each individual component; though relative binding and neutralization titers
255 varied between immunogens; this is likely a consequence of length and/or composition. Further
256 oligomerization for increased multivalent display was accomplished by conjugating two 4mer
257 BOAS inclusive of eight distinct HA heads to a ferritin nanoparticle via SpyTag/SpyCatcher
258 ligation. Similar to the BOAS, these conjugated nanoparticles elicited similar titers to all eight HA
259 components and could neutralize matched viruses.

260

261 Thus, tandemly linking HA heads is a robust method for displaying multiple influenza subtypes in
262 a single protein-based immunogen. Binding titers were elicited to all components present in the
263 immunogen, and there was no significant correlation between HA position within the BOAS (*i.e.,*
264 terminal or internal) and immunogenicity. However, relative immunogenicities of each HA varied
265 despite the guaranteed equimolar display of each subtype. There were qualitatively
266 immunodominant HAs, notably H4 and H9, and these were relatively consistent across BOAS in
267 which they were a component. This effect was reduced in the mix cohort. Further studies using the
268 modularity of the BOAS could further deconvolute relative immunodominances of HA subtypes.
269

270 Despite similar binding titers across multiple BOAS lengths, expression levels and neutralization
271 titers were quite variable. While all 3mer to 8mer BOAS could be overexpressed, expression
272 inversely correlated with overall length. To mitigate this, multiple BOAS (*e.g.,* two 4mers) or
273 conjugation to protein-based nanoparticles, as was done here, could be used to ensure coverage of
274 each desired HA subtype. Furthermore, neutralization titers were quite variable across different
275 BOAS lengths despite similar binding titers. This may be related to multiple factors including
276 homology, stability, and accessibility of neutralizing epitopes for different BOAS lengths.
277 Notably, for longer BOAS we observed degradation following longer term storage at 4C, which
278 may reflect their overall stability. Studies manipulating BOAS composition at intermediate lengths
279 could optimize neutralizing responses to particular influenzas of interest.
280

281 Based on the immunogenicity of the various BOAS and their ability to elicit neutralizing
282 responses, it may not be necessary to maximize the number of HA heads into a single immunogen.
283 Indeed, it qualitatively appears that the intermediate 4-, 5-, and 6mer BOAS were the most
284 immunogenic and this length may be sufficient to effectively engage and crosslink BCR for potent
285 stimulation. These BOAS also had similar or improved binding cross-reactivity to mis-matched
286 HAs as compared to longer 7- or 8mer BOAS. Notably, the 3mer BOAS elicited detectable cross-
287 reactive binding titers to H4 and H5 mismatched HAs in all mice. This observed cross-reactivity
288 could be due to sequence conservation between the HAs, as H3 and H4 share ~51% sequence
289 identity, and H1 and H2 share ~46% and ~62% overall sequence identity with H5, respectively
290 (**Supplemental Figure 7**). Additionally, the degree of surface conservation decreased

291 considerably beyond the 5mer as more antigenically distinct HAs were added to the BOAS. These
292 data suggest that both antigenic distance between HA components and BOAS length play a key
293 role in eliciting cross-reactive antibody responses, and further studies are necessary to optimize
294 BOAS valency and antigenic distance for a desired response.
295
296 Potential enrichment of antibodies targeting the conserved RBS and TI epitopes may also be
297 contributing to observed cross-reactivity. Both epitopes are relatively conserved across all BOAS
298 lengths (**Figure 4C**), and the two BOAS showing the most cross-reactivity, the 3mer and 5mer,
299 elicit a significant portion of the serum response toward both RBS and TI epitopes as determined
300 via a serum competition assay with available epitope-directed antibodies (**Figure 4B**). Notably,
301 this proportion is approximate, as at the time of reporting, antibodies that bind the receptor binding
302 site of all components were not available. RBS-directed antibodies to the H4 and H9 component
303 were not available, and the RBS-directed antibodies used targeting the other HA components have
304 different footprints around the periphery of the RBS. Additionally, there are currently no reported
305 influenza B TI-directed antibodies in the literature. Therefore, this may be an underestimate of the
306 serum proportion focused to the conserved RBS and TI epitopes. Isolated TI-directed antibodies,
307 in particular, can engage more than nine unique subtypes across both group 1 and 2 influenzas[10,12],
308 and our monomeric head-based BOAS immunogens, have the otherwise occluded TI epitope
309 exposed[10–12]. Furthermore, we have previously shown that this TI epitope, when exposed, is
310 immunodominant in the murine model[14]. Further studies with different combinations of HAs could
311 aid in understanding how length and composition influences epitope focusing. For example, a
312 BOAS design with a cluster of group 1 HAs followed by a cluster of group 2 HAs, rather than our
313 roughly alternating pattern could impact which HAs are in close proximity to one other or could
314 be potentially shielded in certain conformations, and thus could affect antigenic results. Combining
315 the BOAS platform with other immune-focusing approaches[32] such as hyperglycosylation[14,31,61,62]
316 or resurfacing[30,63] could enhance cross-reactive responses. Additionally, modifying linker spacing
317 and rigidity can also be used as a mechanism to enhance BCR cross-linking and thus enhance
318 cross-reactive B cell activation and elicitation[64].
319
320 BOAS can be further multimerized via conjugation to a surface of a nanoparticle. Interestingly,
321 this only had a marginal effect on immunogenicity. The BOAS conjugated-nanoparticle elicited

322 titers of ~10^5 (**Figure 6B**), whereas the best BOAS alone reached an order of magnitude greater
323 (**Fig 3C**). This appears in contrast with other studies where attaching an antigen to a nanoparticle
324 scaffold enhanced immunogenicity and neutralization potency[38,65–68]. One recent example
325 designed quartets of antigenically distinct SARS-like betacoronavirus RBDs coupled to an mi3-
326 VLP scaffold via a similar SpyCatchter/SpyTag system and showed increased binding and
327 neutralization titers following conjugation to the NP compared to quartet alone[48]. This discrepancy
328 may be in part due to the larger mi3 nanoparticle[69] which displays 60 copies of the antigen rather
329 than the 24 copies displayed on the ferritin nanoparticle used in this study. Nevertheless, HA-
330 specific responses were similar whether the BOAS were conjugated to the nanoparticle or not,
331 indicating that HA proximity to the NP surface did not impact responses to each component. This
332 observation is consistent with betacoronavirus quartet nanoparticles as well. Additionally, BOAS
333 conjugation to the nanoparticle significantly reduced the scaffold-directed response to near
334 baseline. The addition of the large BOAS projections to the surface of the nanoparticle likely
335 masked the immunogenic scaffold epitopes[70].
336
337 Collectively, this study demonstrates the versatility of the BOAS platform to present multiple HA
338 subtypes as a single immunogen. This "plug-and-play" approach can readily exchange HAs to
339 elicit desired immune responses. BOAS are potentially advantageous over other multivalent
340 display platforms such as protein-based nanoparticles, which can produce off-target responses due
341 to their inherent immunogenicity[38]. Furthermore, when genetic fusions of the antigen to
342 nanoparticles is not possible, SpyCatcher/SpyTag (or another suitable conjugation approach) must
343 be used, further contributing to scaffold-specific responses as well as additional multi-step
344 manufacturing and purification challenges. Not only does our BOAS platform circumvent these
345 potential caveats, but because this is a single polypeptide chain, this immunogen could readily be
346 formulated as an mRNA lipid nanoparticle (LNP)[71]. The BOAS platform forms the basis for next-
347 generation influenza vaccines and can more broadly be readily adapted to other viral antigens.

348 **MATERIALS AND METHODS**

349 **Beads-on-a-string (BOAS) immunogen and full-length hemagglutinin (HA) expression and**
350 **purification**

351 Hemagglutinin (HA) head for BOAS immunogens were designed based on the following
352 sequences from the following subtypes: H1 (H1/A/Michigan/45/2015) (GenBank: AMA11475.1) ,
353 H2 (H2/A/Japan/305/1957) (GenBank: AAA43185), H3 (H3/A/Kansas/14/2017) (GenBank:
354 AVG71503), H4 (H4/A/American Black Duck/New Brunswick/00464/2010) (GenBank:
355 AGG81749), H5 (H5/A/Viet Nam/1203/2004) (GenBank: ADD97095), H7
356 (H7/A/Shanghai/01/2014) (GenBank: AHK10800), H9 (H9/A/Guangdong/MZ058/2016)
357 (GenBank: AOR17625.1), and B (B/Malaysia/2506/2004) (GenBank: ABU99194). Head
358 subdomains from these HAs were used in the BOAS immunogens, and full-length soluble
359 ectodomain (FLsE) trimers were used in ELISAs. Additional H1 (H1/A/Solomon Islands/3/2006)
360 and H3 (H3/A/Hong Kong/1/1968) FLsEs were used in ELISAs as mismatched, antigenically
361 distinct HAs for all BOAS. Sequences were codon optimized using IDT and subcloned into pVRC
362 vectors for expression in mammalian cells. For BOAS immunogens, all HA heads were separated
363 by a "GA$(GSS)_4$AS" spacer. Specific head domain regions for each subtype were selected based
364 on expression levels in expi293F cells. All protein sequences contained a C-terminal 8x-His tag
365 for purification with an upstream 3C-protease cleavage site. Full-length HA trimers contained an
366 additional C-terminal foldon (Fd) trimerization domain for expression as soluble trimers. BOAS
367 immunogens and HA trimers were transfected in expi293F cells using Expifectamine transfection
368 reagent and enhancers based on manufacturer's instructions. Five days post-transfection,
369 supernatant was harvested and clarified via centrifugation, then purified on a TALON cobalt resin
370 via the 8x-His Tag. Recovered proteins were then purified on a Superdex 200 (S200) Increase
371 10/300 GL (for trimeric HAs) or Superose 6 Increase 10/300 GL (for BOAS) size-exclusion
372 column in Dulbecco's Phosphate Buffered Saline (DPBS) within 48 hours of cobalt resin elution.
373 Pooled fractions of BOAS were then treated with HRV-3C protease to remove tags for 16 hours
374 at 4°C, then passed over a TALON cobalt resin to remove any remaining protease, cleaved tags,
375 and uncleaved protein. Trimeric HAs were used for ELISAs with purification tags present.

376

377 **IgG expression and purification**

378 All antibody variable regions were codon optimized for mammalian cell expression and subcloned
379 into pVRC vectors containing either heavy or light (kappa or lambda) with humanized constant
380 regions. Equimolar heavy and light chain plasmids were co-transfected into HEK293F cells using
381 polyethylenimine (PEI). Five days following transfection, supernatants were harvested, clarified
382 via centrifugation, and purified on a Protein G resin. Purified antibodies were then buffer
383 exchanged into DPBS for use in ELISA assays.
384
385 **Nanoparticle Assembly**
386 C-terminally SpyTagged BOAS and N-terminal SpyCatcher nanoparticles were subcloned into
387 pVRC expression vectors, then expressed in expi293F cells and purified via TALON cobalt resin
388 as above. SpyTagged BOAS were further purified via size-exclusion chromatography on a
389 Superose 6 column, as above, followed by cleavage of the C-terminal His tag via 3C HRV protease
390 to yield a C-terminal SpyTag. SpyCatcher nanoparticles were purified on a HiPrep Sephacryl S400
391 column in DPBS. Purified SpyCatcher nanoparticles was when mixed with an equimolar ratio
392 mixture of each 4mer BOAS (H1, H2, H3, H4 and H5, H7, H9,B) at a 1.2 molar excess relative to
393 the nanoparticle overnight at 4°C. The mixture was then re-purified over an S400 column,
394 concentrated, aliquoted, and snap-frozen in liquid nitrogen until use.
395
396 **Negative Staining procedure for TEM**
397 5µl of the sample was adsorbed for 1 minute onto a carbon-coated grid made hydrophilic by a 20
398 second exposure to a glow discharge (25mA). Excess liquid was removed with filter paper
399 (Whatman #1), the grid was then floated briefly on a drop of water (to wash away phosphate or
400 salt), blotted again on a filer paper and then stained with 0.75% uranyl formate or 1% uranyl acetate
401 for 20-30 seconds. After removing the excess stain with a filter paper the grids were examined in
402 a JEOL 1200EX Transmission electron microscope or a TecnaiG² Spirit BioTWIN and images
403 were recorded with an AMT 2k CCD camera.
404
405 **Immunizations**
406 C57BL/6 mice (Jackson Laboratory) (n=8 per group for 3-, 4-, 5-, 6-, 7-, and 8mer cohorts; n=5
407 for BOAS NP, NP, and mix cohorts) were immunized with 20µg of BOAS immunogens of varying
408 length and adjuvanted with 50% Sigmas Adjuvant for a total of 100µL of inoculum. Immunogens

409 and adjuvant were administered intramuscularly (IM) at day 0, day 14, and day 28. Serum samples
410 were collected at days 0, 14, 28, and 42 (prior to immunogen administration). All experiments
411 were conducted in 6-10 week old female mice under the institutional IACUC protocol
412 (2014N000252).
413
414 **Serum ELISAs**
415 High-binding 96-well plates (Corning) were coated with 200ng per well of BOAS immunogen,
416 nanoparticle, or trimeric HAs overnight at 4°C in DPBS. The following day, plates were blocked
417 with 1% BSA in PBS-T (DPBS+0.1% Tween-20) for 1 hour at RT, rocking. Diluted serum in
418 DPBS were generated starting at a 1:50 dilution, followed by 10-fold serial dilutions for a total of
419 7 dilutions. After one hour, blocking buffer was discarded, and 40µL of diluted serum was added
420 and incubated for 1 hour at RT, rocking. Serum was then discarded, and plates were washed 3
421 times with PBS-T, after which 100µL of HRP-conjugated anti-mouse secondary antibody (Abcam)
422 at a 1:20,000 dilution was added and incubated for 1 hour at RT rocking. Following secondary
423 antibody incubation, plates were again washed 3 times with PBS-T. Slow TMB development
424 solution was then added to plates and incubated for 30-40 mins at RT, then stopped with an equal
425 volume of 0.2M sulfuric acid stop solution. Developed plates were then analyzed via absorbance
426 measurements at 450nm. Each condition was blank subtracted with a secondary only control and
427 plotted in GraphPad Prism 10 (v10.0.2). Serum endpoint titer (EPT) were determined using a non-
428 linear regression (sigmoidal, four-parameter logistic (4PL) equation, where x is concentration) to
429 determine the dilution at which dilution the blank-subtracted 450nm absorbance value intersect a
430 0.1 threshold. Serum titers for individual mice against respective antigens are reported as log
431 transformed values of the EPT dilution.
432
433 **Serum Competition ELISAs**
434 Serum competition ELISAs were performed following a similar protocol to serum ELISAs
435 described above. Following blocking with BSA in PBS-T, blocking solution was discarded and
436 40µL of either DPBS (no competition control), a cocktail of humanized antibodies targeting the
437 RBS and periphery (5J8, 2G1, K03.12, H5.3, H7.167, H1209), a cocktail of humanized TI-directed
438 antibodies (S5V2-29, D1 H1-17/H3-14, D2 H1-1/H3-1), or a negative control antibody
439 (MEDI8852) were added at a concentration of 100µg/mL per antibody. Plates were incubated with

440 competing antibodies or controls for 1 hour at RT. Serum from mice from respective BOAS
441 cohorts were diluted by 1:5,000 (3mer and 6mer) or 1:10,000 (4mer, 5mer, 7mer, and 8mer) in
442 DPBS, then 40µL added on top of competing antibody for a final dilution of 1:10,000 (3mer and
443 6mer) or 1:20,000 (4mer, 5mer, 7mer, and 8mer). These dilutions were selected based on a dilution
444 range in serum ELISAs in which serum reactivity behaved linearly. Plates were incubated with
445 serum and competing antibodies for an additional 1 hour at RT, washed 3 times with PBS-T, then
446 incubated with an HRP-conjugated human/bovine/horse cross-adsorbed anti-mouse secondary
447 antibody (Southern Biotech) at a 1:20,000 dilution for 1 hour at RT. The remaining wash and
448 development steps were performed as in the serum ELISA.
449
450 **Microneutralization Assays**
451 Serum microneutralization assays using R3 viruses followed the published protocol in Creanga et
452 al[51]. Briefly, MDCK-SIAT1-PB1/H5/H7 cells were thawed into D10 media with penicillin and
453 streptomycin (P/S) and 10% heat-inactivated fetal bovine serum (FBS) three days prior to
454 infection. Cells were seeded two days later at $1.5x10^4$ cells/well in flu media (Opti-MEM + 0.01%
455 FBS + P/S + 0.3% Bovine Serum Albumin (BSA) + Ca/Mg) overnight at 37°C. Serum was also
456 treated with receptor destroying enzyme (RDE) II at a 1:3 dilution overnight at 37°C, followed by
457 inactivation at 56°C for 30-60 mins. Treated serum was then diluted in media at 1:3 for a final
458 starting dilution of 1:32. On the day of infection, cells were treated with 60µL of virus in flu media
459 + TPCK-trypsin for 1 hour at 37°C with 5% CO_2. After one hour, media was removed via
460 aspiration and cells were treated with 100µL treated serum. The following day, fluorescent foci
461 were counted on a Zeiss Celldiscoverer 7 + LSM900 + Airyscan 2 (CD7+LSM900) to determine
462 neutralization. Counts were normalized to a cell control and untreated virus control, and IC50
463 values for neutralization were determined via a fit to a 4PL non-linear regression in technical
464 duplicate in Prism v10.0.2 (GraphPad).
465
466 **Homology Analyses**
467 Homology analyses on HA BOAS was conducted using a manual method analogous to
468 Consurf[59,60]. HA head domain structures (or closely related variants) were aligned in Pymol to the
469 H2 JP-57 structure (PDB: 2WRE). Structures used for alignments were as follows: H1 (PDB:
470 6XGC), H3 (PDB: 4O5N), H4 (PDB: 5XL3), H5 (PDB: 6CFG), H7 (PDB: 6FYU), H9 (PDB:

471 1JSI), B (PDB: 4FQJ). Any mis-matches in specific amino acids were adjusted using the
472 mutagenesis wizard in Pymol. Following structural alignment, each position on the HA head
473 domain was scored for % aa identity at each position on a scale of 1-9, where 1 = 10-19% identical,
474 2 = 20-29% identical … to 9 = 90-100% identical, which we refer to as a "conservation score".
475 This was repeated for each composition of BOAS (i.e. 3mer, 4mer, 5mer, … 8mer). Each position
476 on the H2 structure was then pseudo colored based on the conservation score. Average amino acid
477 conservation scores were defined as the average of conservation score over the whole sequence
478 (overall), or of amino acids within a given epitope. TI epitope amino acids were defined as residues
479 60, 86-106, and 212-232 (H1 numbering), and RBS epitope amino acids were defined as residues
480 94-96, 128-146, 153-161, 182-194, and 222-229 (H1 numbering).
481
482 **Statistical Analysis**
483 Significance for ELISAs and microneutralization assays were determined using Prism (GraphPad
484 Prism v10.2.3). ELISAs comparing serum reactivity and microneutralization and comparing >2
485 samples were analyzed using a Kruskal-Wallis test with Dunn's post-hoc test to correct for
486 multiple comparisons. Multiple comparisons were made between each possible combination or
487 relative to a control group, where indicated. ELISAs comparing two samples were analyzed using
488 a Mann-Whitney test. Significance was assigned with the following: * = $p<0.05$, ** = $p<0.01$,
489 *** = $p<0.001$, and **** = $p<0.0001$. Where conditions are compared and no significance is
490 reported, the difference was non-significant.
491
492 **ACKNOWLEDGMENTS**
493 We thank the mouse facility at the Ragon Institute for mouse maintenance. We also thank Nicholas
494 Lamson for helping with DLS measurements for nanoparticle characterization. We would like to
495 also thank Maria Ericcson for acquiring NS-EM images. We acknowledge support from R01
496 AI146779 and P01 AI089618 (AGS) and R01AI137057, R01AI153098, and R01AI155447 (DL).
497 This research has been funded in whole or part with federal funds under a contract from the
498 National Institute of Allergy and Infectious Diseases, NIH contract 75N93019C00050 (AGS).
499
500 **AUTHOR INFORMATION**
501

502 **Author Contributions:**

503 DTL and AGS designed research; DTL, FAMN, MLV, DPM, and LR performed research; DTL
504 and AGS analyzed data; DTL and AGS wrote the paper. All authors edited and commented on the
505 paper.

506

507 **Correspondence and requests for materials should be addressed to:** Aaron G. Schmidt
508 (aschmidt@crystal.harvard.edu)

509

510 **Competing financial interest:** DTL and AGS have filed a provisional patent covering the work
511 described here.

512 **REFERENCES**

513

514 1. Wei, C.-J. *et al.* Next-generation influenza vaccines: opportunities and challenges. *Nat Rev*
515 *Drug Discov* **19**, 239–252 (2020).

516 2. Raymond, D. D. *et al.* Influenza immunization elicits antibodies specific for an egg-adapted
517 vaccine strain. *Nature Medicine* **22**, 1465–1469 (2016).

518 3. Ekiert, D. C. *et al.* Cross-neutralization of influenza A viruses mediated by a single antibody
519 loop. *Nature* **489**, 526–532 (2012).

520 4. Hong, M. *et al.* Antibody recognition of the pandemic H1N1 Influenza virus hemagglutinin
521 receptor binding site. *Journal of Virology* **87**, 12471–12480 (2013).

522 5. Krause, J. C. *et al.* Human Monoclonal Antibodies to Pandemic 1957 H2N2 and Pandemic
523 1968 H3N2 Influenza Viruses. *J. Virol.* **86**, 6334–6340 (2012).

524 6. Krause, J. C. *et al.* A broadly neutralizing human monoclonal antibody that recognizes a
525 conserved, novel epitope on the globular head of the influenza H1N1 virus hemagglutinin.
526 *Journal of Virology* **85**, 10905–10908 (2011).

527 7. Lee, P. S. *et al.* Receptor mimicry by antibody F045-092 facilitates universal binding to the
528 H3 subtype of influenza virus. *Nature Communications* **5**, 3614–9 (2014).

529 8. Lee, P. S. *et al.* Heterosubtypic antibody recognition of the influenza virus hemagglutinin
530 receptor binding site enhanced by avidity. *Proc National Acad Sci* **109**, 17040–17045 (2012).

531 9. Schmidt, A. G. *et al.* Preconfiguration of the antigen-binding site during affinity maturation of
532 a broadly neutralizing influenza virus antibody. *Proceedings of the National Academy of*
533 *Sciences of the United States of America* **110**, 264–269 (2013).

534 10. McCarthy, K. R. *et al.* A Prevalent Focused Human Antibody Response to the Influenza
535 Virus Hemagglutinin Head Interface. *Mbio* **12**, e01144-21 (2021).

536 11. Bangaru, S. *et al.* A Site of Vulnerability on the Influenza Virus Hemagglutinin Head
537 Domain Trimer Interface. *Cell* **177**, 1136-1152.e18 (2019).

538 12. Watanabe, A. *et al.* Antibodies to a Conserved Influenza Head Interface Epitope Protect by
539 an IgG Subtype-Dependent Mechanism. *Cell* **177**, 1124-1135.e16 (2019).

540 13. Dong, J. *et al.* Anti–influenza H7 human antibody targets antigenic site in hemagglutinin
541 head domain interface. *J Clin Invest* **130**, 4734–4739 (2020).

542 14. Bajic, G. *et al.* Influenza Antigen Engineering Focuses Immune Responses to a Subdominant
543 but Broadly Protective Viral Epitope. *Cell Host Microbe* **25**, 827-835.e6 (2019).

544 15. Corti, D. *et al.* A Neutralizing Antibody Selected from Plasma Cells that Binds to Group 1
545 and Group 2 Influenza A Hemagglutinins. *Science* **333**, 850–856 (2011).

546 16. Dreyfus, C., Ekiert, D. C. & Wilson, I. A. Structure of a classical broadly neutralizing stem
547 antibody in complex with a pandemic H2 influenza virus hemagglutinin. *Journal of Virology* **87**,
548 7149–7154 (2013).

549 17. Dreyfus, C. *et al.* Highly conserved protective epitopes on influenza B viruses. *Science* **337**,
550 1343–1348 (2012).

551 18. Ekiert, D. C. *et al.* Antibody Recognition of a Highly Conserved Influenza Virus Epitope.
552 *Science* **324**, 246–251 (2009).

553 19. Friesen, R. H. E. *et al.* A common solution to group 2 influenza virus neutralization. *Proc.*
554 *Natl. Acad. Sci.* **111**, 445–450 (2014).

555 20. Kallewaard, N. L. *et al.* Structure and Function Analysis of an Antibody Recognizing All
556 Influenza A Subtypes. *Cell* **166**, 596–608 (2016).

557 21. Caradonna, T. M. & Schmidt, A. G. Protein engineering strategies for rational immunogen
558 design. *Npj Vaccines* **6**, 154 (2021).

559 22. Impagliazzo, A. *et al.* A stable trimeric influenza hemagglutinin stem as a broadly protective
560 immunogen. *Science* **349**, 1301–1306 (2015).

561 23. Yassine, H. M. *et al.* Hemagglutinin-stem nanoparticles generate heterosubtypic influenza
562 protection. *Nature Medicine* **21**, 1065–1070 (2015).

563 24. Nachbagauer, R. *et al.* A chimeric hemagglutinin-based universal influenza virus vaccine
564 approach induces broad and long-lasting immunity in a randomized, placebo-controlled phase I
565 trial. *Nature Medicine* 1–20 (2020) doi:10.1038/s41591-020-1118-7.

566 25. Giles, B. M. & Ross, T. M. A computationally optimized broadly reactive antigen (COBRA)
567 based H5N1 VLP vaccine elicits broadly reactive antibodies in mice and ferrets. *Vaccine* **29**,
568 3043–3054 (2011).

569 26. Skarlupka, A. L., Reneer, Z. B., Abreu, R. B., Ross, T. M. & Sautto, G. A. An Influenza
570 Virus Hemagglutinin Computationally Optimized Broadly Reactive Antigen Elicits Antibodies
571 Endowed with Group 1 Heterosubtypic Breadth against Swine Influenza Viruses. *J. Virol.* **94**,
572 (2020).

573 27. Reneer, Z. B., Jamieson, P. J., Skarlupka, A. L., Huang, Y. & Ross, T. M. Computationally
574 Optimized Broadly Reactive H2 HA Influenza Vaccines Elicited Broadly Cross-Reactive
575 Antibodies and Protected Mice from Viral Challenges. *J. Virol.* **95**, (2020).

576 28. Wong, T. M. *et al.* Computationally Optimized Broadly Reactive Hemagglutinin Elicits
577 Hemagglutination Inhibition Antibodies against a Panel of H3N2 Influenza Virus Cocirculating
578 Variants. *J. Virol.* **91**, (2017).

579 29. Carter, D. M. *et al.* Design and Characterization of a Computationally Optimized Broadly
580 Reactive Hemagglutinin Vaccine for H1N1 Influenza Viruses. *J. Virol.* **90**, 4720–4734 (2016).

581 30. Bajic, G. *et al.* Structure-Guided Molecular Grafting of a Complex Broadly Neutralizing
582 Viral Epitope. *Acs Infect Dis* **6**, 1182–1191 (2020).

583 31. Thornlow, D. N. *et al.* Altering the Immunogenicity of Hemagglutinin Immunogens by
584 Hyperglycosylation and Disulfide Stabilization. *Front Immunol* **12**, 737973 (2021).

585 32. Dosey, A. *et al.* Combinatorial immune refocusing within the influenza hemagglutinin head
586 elicits cross-neutralizing antibody responses. *bioRxiv* 2023.05.23.541996 (2023)
587 doi:10.1101/2023.05.23.541996.

588 33. Bachmann, M. F. & Jennings, G. T. Vaccine delivery: a matter of size, geometry, kinetics
589 and molecular patterns. *Nat. Rev. Immunol.* **10**, 787–796 (2010).

590 34. Nguyen, B. & Tolia, N. H. Protein-based antigen presentation platforms for nanoparticle
591 vaccines. *npj Vaccines* **6**, 70 (2021).

592 35. Curley, S. M. & Putnam, D. Biological Nanoparticles in Vaccine Development. *Front.*
593 *Bioeng. Biotechnol.* **10**, 867119 (2022).

594 36. Bachmann, M. F. & Jennings, G. T. Vaccine delivery: a matter of size, geometry, kinetics
595 and molecular patterns. *Nat. Rev. Immunol.* **10**, 787–796 (2010).

596 37. Joyce, M. G. *et al.* A SARS-CoV-2 ferritin nanoparticle vaccine elicits protective immune
597 responses in nonhuman primates. *Sci. Transl. Med.* **14**, eabi5735 (2021).

598 38. Kanekiyo, M. *et al.* Self-assembling influenza nanoparticle vaccines elicit broadly
599 neutralizing H1N1 antibodies. *Nature* **498**, 102–106 (2013).

600 39. Georgiev, I. S. *et al.* Two-Component Ferritin Nanoparticles for Multimerization of Diverse
601 Trimeric Antigens. *ACS Infectious Diseases* **4**, 788–796 (2018).

602 40. He, L. *et al.* Presenting native-like trimeric HIV-1 antigens with self-assembling
603 nanoparticles. *Nat. Commun.* **7**, 12041 (2016).

604 41. Kanekiyo, M. *et al.* Mosaic nanoparticle display of diverse influenza virus hemagglutinins
605 elicits broad B cell responses. *Nature Immunology* 1–18 (2019) doi:10.1038/s41590-018-0305-x.

606 42. McLeod, B. *et al.* Vaccination with a structure-based stabilized version of malarial antigen
607 Pfs48/45 elicits ultra-potent transmission-blocking antibody responses. *Immunity* (2022)
608 doi:10.1016/j.immuni.2022.07.015.

609 43. Kanekiyo, M. *et al.* Rational Design of an Epstein-Barr Virus Vaccine Targeting the
610 Receptor-Binding Site. *Cell* **162**, 1090–1100 (2015).

611 44. Cohen, A. A. *et al.* Construction, characterization, and immunization of nanoparticles that
612 display a diverse array of influenza HA trimers. *Plos One* **16**, e0247963 (2021).

613 45. Boyoglu-Barnum, S. *et al.* Quadrivalent influenza nanoparticle vaccines induce broad
614 protection. *Nature* 1–6 (2021) doi:10.1038/s41586-021-03365-x.

615 46. Zhao, H. *et al.* Induction of Neutralizing Antibodies against Four Serotypes of Dengue
616 Viruses by MixBiEDIII, a Tetravalent Dengue Vaccine. *PLoS ONE* **9**, e86573 (2014).

617 47. Etemad, B. *et al.* An envelope domain III-based chimeric antigen produced in Pichia pastoris
618 elicits neutralizing antibodies against all four dengue virus serotypes. *Am. J. Trop. Med. Hyg.* **79**,
619 353–63 (2008).

620 48. Hills, R. A. *et al.* Proactive vaccination using multiviral Quartet Nanocages to elicit broad
621 anti-coronavirus responses. *Nat. Nanotechnol.* 1–8 (2024) doi:10.1038/s41565-024-01655-9.

622 49. Cohen, A. A. *et al.* Mosaic nanoparticles elicit cross-reactive immune responses to zoonotic
623 coronaviruses in mice. *Sci New York N Y* **371**, 735–741 (2021).

624 50. Cohen, A. A. *et al.* Mosaic RBD nanoparticles protect against challenge by diverse
625 sarbecoviruses in animal models. *Science* (2022) doi:10.1126/science.abq0839.

626 51. Creanga, A. *et al.* A comprehensive influenza reporter virus panel for high-throughput deep
627 profiling of neutralizing antibodies. *Nat Commun* **12**, 1722 (2021).

628 52. Zakeri, B. *et al.* Peptide tag forming a rapid covalent bond to a protein, through engineering a
629 bacterial adhesin. *Proc. Natl. Acad. Sci.* **109**, E690–E697 (2012).

630 53. Sutherland, A. R., Alam, Md. K. & Geyer, C. R. Post-translational Assembly of Protein Parts
631 into Complex Devices by Using SpyTag/SpyCatcher Protein Ligase. *ChemBioChem* **20**, 319–328
632 (2019).

633 54. McCarthy, K. R. *et al.* Memory B Cells that Cross-React with Group 1 and Group 2
634 Influenza A Viruses Are Abundant in Adult Human Repertoires. *Immunity* **48**, 174-183.e9
635 (2018).

636 55. Caradonna, T. M. *et al.* An epitope-enriched immunogen expands responses to a conserved
637 viral site. *Cell Rep.* **41**, 111628 (2022).

638 56. Winarski, K. L. *et al.* Vaccine-elicited antibody that neutralizes H5N1 influenza and variants
639 binds the receptor site and polymorphic sites. *Proceedings of the National Academy of Sciences*
640 *of the United States of America* **112**, 9346–9351 (2015).

641 57. Thornburg, N. J. *et al.* H7N9 influenza virus neutralizing antibodies that possess few somatic
642 mutations. *J Clin Invest* **126**, 1482–1494 (2016).

643 58. Bajic, G. & Harrison, S. C. Antibodies That Engage the Hemagglutinin Receptor-Binding
644 Site of Influenza B Viruses. *Acs Infect Dis* **7**, 1–5 (2020).

645 59. Glaser, F. *et al.* ConSurf: Identification of Functional Regions in Proteins by Surface-
646 Mapping of Phylogenetic Information. *Bioinformatics* **19**, 163–164 (2003).

647 60. Ashkenazy, H. *et al.* ConSurf 2016: an improved methodology to estimate and visualize
648 evolutionary conservation in macromolecules. *Nucleic Acids Res.* **44**, W344–W350 (2016).

649 61. Ingale, J. *et al.* Hyperglycosylated Stable Core Immunogens Designed To Present the CD4
650 Binding Site Are Preferentially Recognized by Broadly Neutralizing Antibodies. *J Virol* **88**,
651 14002–14016 (2014).

652 62. Eggink, D., Goff, P. H. & Palese, P. Guiding the Immune Response against Influenza Virus
653 Hemagglutinin toward the Conserved Stalk Domain by Hyperglycosylation of the Globular Head
654 Domain. *J Virol* **88**, 699–704 (2014).

655 63. Hai, R. *et al.* Influenza viruses expressing chimeric hemagglutinins: globular head and stalk
656 domains derived from different subtypes. *Journal of Virology* **86**, 5774–5781 (2012).

657 64. Veneziano, R. *et al.* Role of nanoscale antigen organization on B-cell activation probed using
658 DNA origami. *Nat. Nanotechnol.* **15**, 716–723 (2020).

659 65. Jardine, J. *et al.* Rational HIV immunogen design to target specific germline B cell receptors.
660 *Science* **340**, 711–716 (2013).

661 66. Tokatlian, T. *et al.* Innate immune recognition of glycans targets HIV nanoparticle
662 immunogens to germinal centers. *Science* **363**, 649–654 (2019).

663 67. Kato, Y. *et al.* Multifaceted Effects of Antigen Valency on B Cell Response Composition
664 and Differentiation In Vivo. *Immunity* **53**, 548-563.e8 (2020).

665 68. Marcandalli, J. *et al.* Induction of Potent Neutralizing Antibody Responses by a Designed
666 Protein Nanoparticle Vaccine for Respiratory Syncytial Virus. *Cell* **176**, 1420-1431.e17 (2019).

667 69. Bruun, T. U. J., Andersson, A.-M. C., Draper, S. J. & Howarth, M. Engineering a Rugged
668 Nanoscaffold To Enhance Plug-and-Display Vaccination. *ACS Nano* **12**, 8855–8866 (2018).

669 70. Kraft, J. C. *et al.* Antigen- and scaffold-specific antibody responses to protein nanoparticle
670 immunogens. *Cell Reports Medicine* 100780 (2022) doi:10.1016/j.xcrm.2022.100780.

671 71. Chaudhary, N., Weissman, D. & Whitehead, K. A. mRNA vaccines for infectious diseases:
672 principles, delivery and clinical translation. *Nat. Rev. Drug Discov.* **20**, 817–838 (2021).

673

674

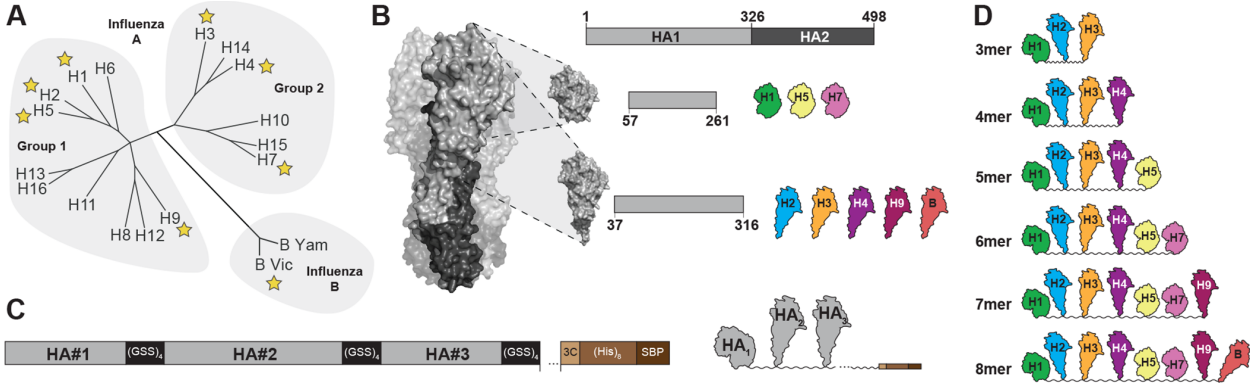

Figure 1: Design of Beads-on-a-string (BOAS) immunogens- (A) Phylogenic tree of influenza hemagglutinin (HA) subtypes. Subtypes are further categorized as group 1, group 2 or influenza B, and stars indicate subtypes included in the BOAS. **(B)** Native trimeric HA structure (A/H3/Hong Kong/1968; PDB: 4FNK) is shown on the left, with the HA1 domain in light grey, and HA2 in dark grey. A construct diagram of full-length HA is shown at the top with the locations of head domain segments within HA1. Head domains of H1, H3, and H7 span residues 57-261, and head domains of H2, H3, H4, H9, and B span 37-316 of the HA1 region of HA. **(C)** Construct diagram of HA BOAS. BOAS are assembled by linking HA head domains (light grey) into a single polypeptide chain where HA head domains are separated by a flexible linker with 4 (GSS) repeats. The C-terminus consists of an HRV-3C protease cleavable His tag and streptavidin-binding-protein (SBP) tag for purification and other affinity tags. **(D)** BOAS used in this study.

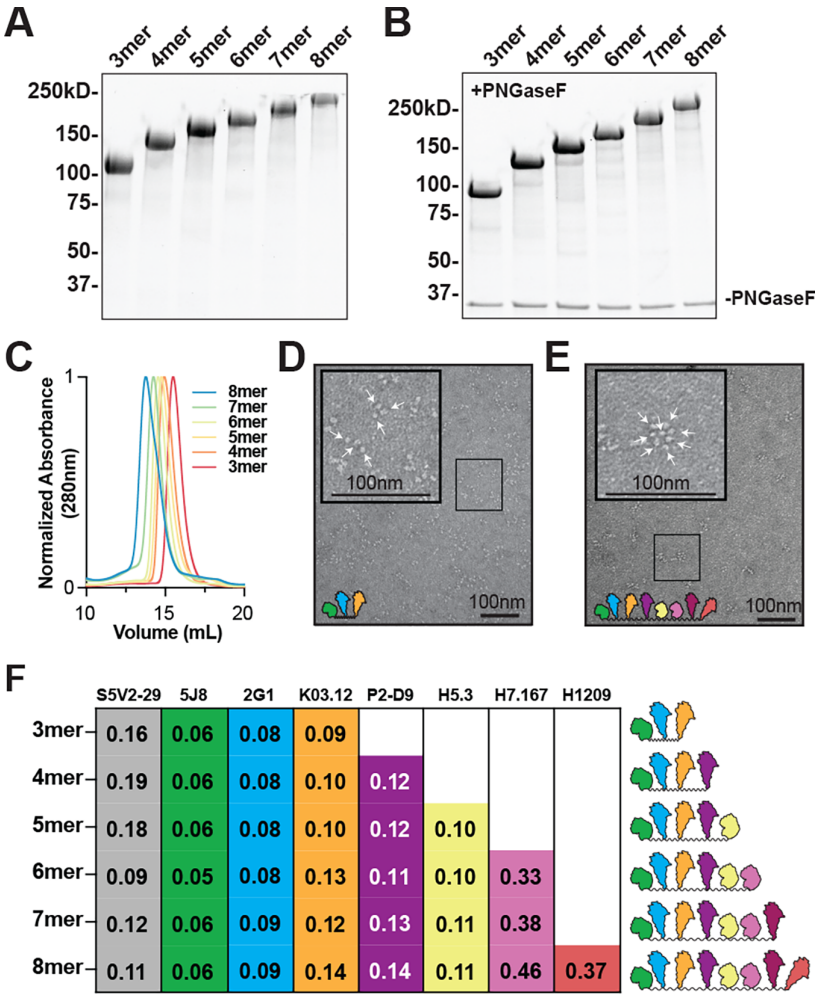

Figure 2: Biochemical Characterization of BOAS- A) SDS-PAGE analysis of 3mer-8mer BOAS under non-reducing conditions. **B)** SDS-PAGE analysis of 3mer-8mer BOAS under non-reducing conditions following glycan digestion with PNGase-F. **C)** Size exclusion chromatography traces of 3mer-8mer BOAS on an Superdex 200 column in PBS. **D)** Negative stain electron microscopy (NS-EM) images of the 3mer. Arrows point to individual HA monomers. Inset image is 2.5X zoomed enlarged image of boxed area. **E)** Negative stain electron microscopy (NS-EM) images of the 8mer. Arrows point to individual HA monomers. Inset image is 2.5X zoomed enlarged image of boxed area. **F)** Characterization via ELISA of BOAS components with subtype-specific antibodies. Apparent K_D values in μM are reported for each antibody for each BOAS immunogen. Antibodies corresponding to each component are as follows: S5V2-29 (interface, all components except B/Mal/04), 5J8 (RBS, H1), 2G1 (RBS, H2), K03.12 (RBS, H3), P2-D9 (H4), H5.3 (RBS, H5), H7.167 (RBS periphery, H7), H1209 (RBS, B).

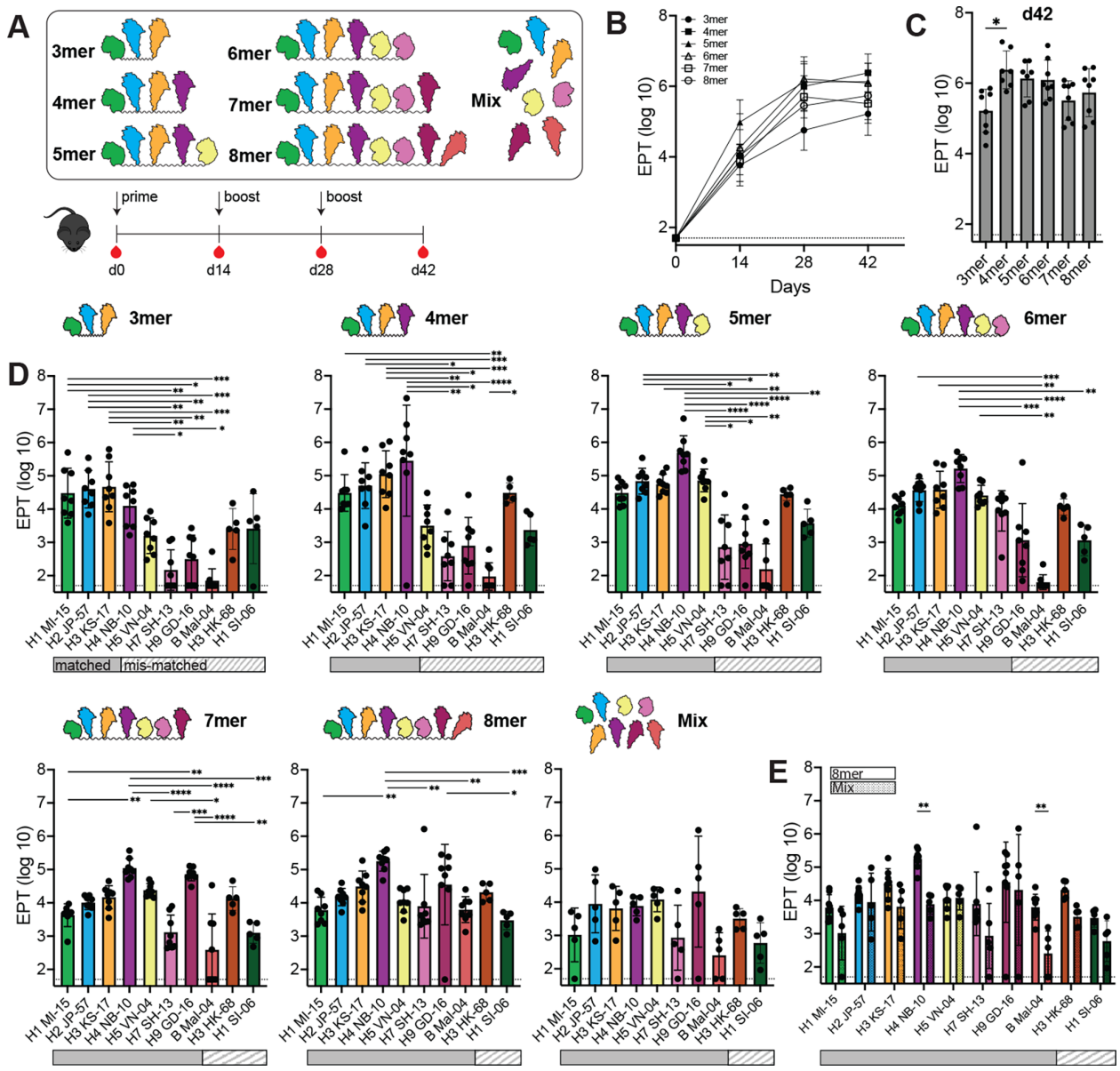

Figure 3: Murine immunizations with 3mer-8mer BOAS- A) Schematic of immunization regimen with 3mer-8mer BOAS and a Mix control containing an equal molar of the 8 individual HA heads not connected with a linker. Mice were primed with 20µg of immunogen, followed by two homologous boosts two weeks apart. **B)** Immunogenicity of BOAS over time as determined by serum ELISA. Serum reactivity to each immunogen is reported as the endpoint titer (EPT) dilution factor for each group (n=8) and d14, d28, and d42. Data points are an average of n=8 mice and error bars are +/- 1 s.d. **C)** Serum titers to each BOAS at the final time point, d42. Data points for single time point antigen titers are from individual mice (n=8, bars represent mean titers and error bars are +/- 1 s.d., * = $p<0.05$ as determined by Kruskal-Wallis test with Dunn's multiple comparison post hoc test relative to the 3mer. **D)** Serum titers to full-length HA trimers elicited by

720 3mer-8mer BOAS. Solid bars below each plot indicate a matched sub-type, and striped bars
721 indicate a mis-matched subtype (i.e. not present in the BOAS). Data points are serum EPTs from
722 individual mice (n=8) and error bars are +/- 1 s.d., * = $p<0.05$, ** = $p<0.01$, *** = $p<0.001$, ****
723 = $p<0.0001$ as determined by a Kruskal-Wallis test with Dunn's multiple comparison post hoc test.
724

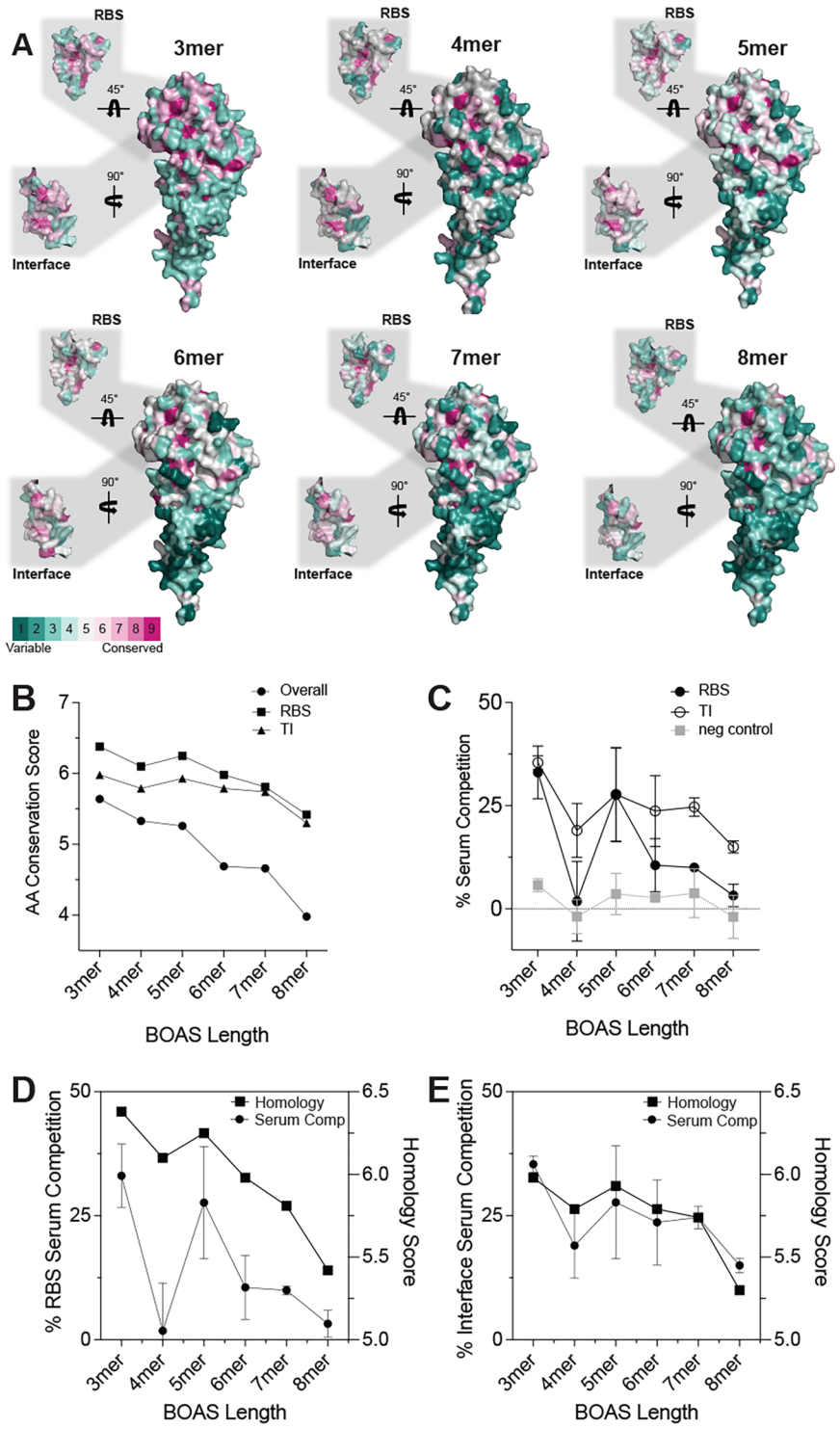

Figure 4: BOAS component epitope homology and serum competition A) Amino acid conservation of each BOAS projected on the A/H2/Japan/1957 head domain structure (PDB: 2WRE). Variability and conservation scores were determined as the % conservation of each

731 residue at each position for each BOAS composition. Cut-outs are RBS and Trimer interface (TI)
732 epitopes with their respective conservation. **B)** Homology score as determined by the average %
733 conservation of each residue across the entire protein sequence (overall, circle), and the RBS
734 (square) and TI (triangle) epitopes. **C)** Serum competition to RBS and TI epitopes as determined
735 via competition with a cocktail of RBS-directed antibodies, TI-directed antibodies, or a stem-
736 directed negative control antibody. % competition is determined by the relative decrease in serum
737 binding to each BOAS normalized to an untreated control. Each data point represents a mean from
738 n=3 mice and error bars are +/- 1 s.d. **D)** Trend overlay of % serum competition with RBS-directed
739 antibodies and homology score of the RBS epitope as a function of BOAS length. **E)** Trend overlay
740 of % serum competition with TI-directed antibodies and homology score of the TI epitope as a
741 function of BOAS length.
742

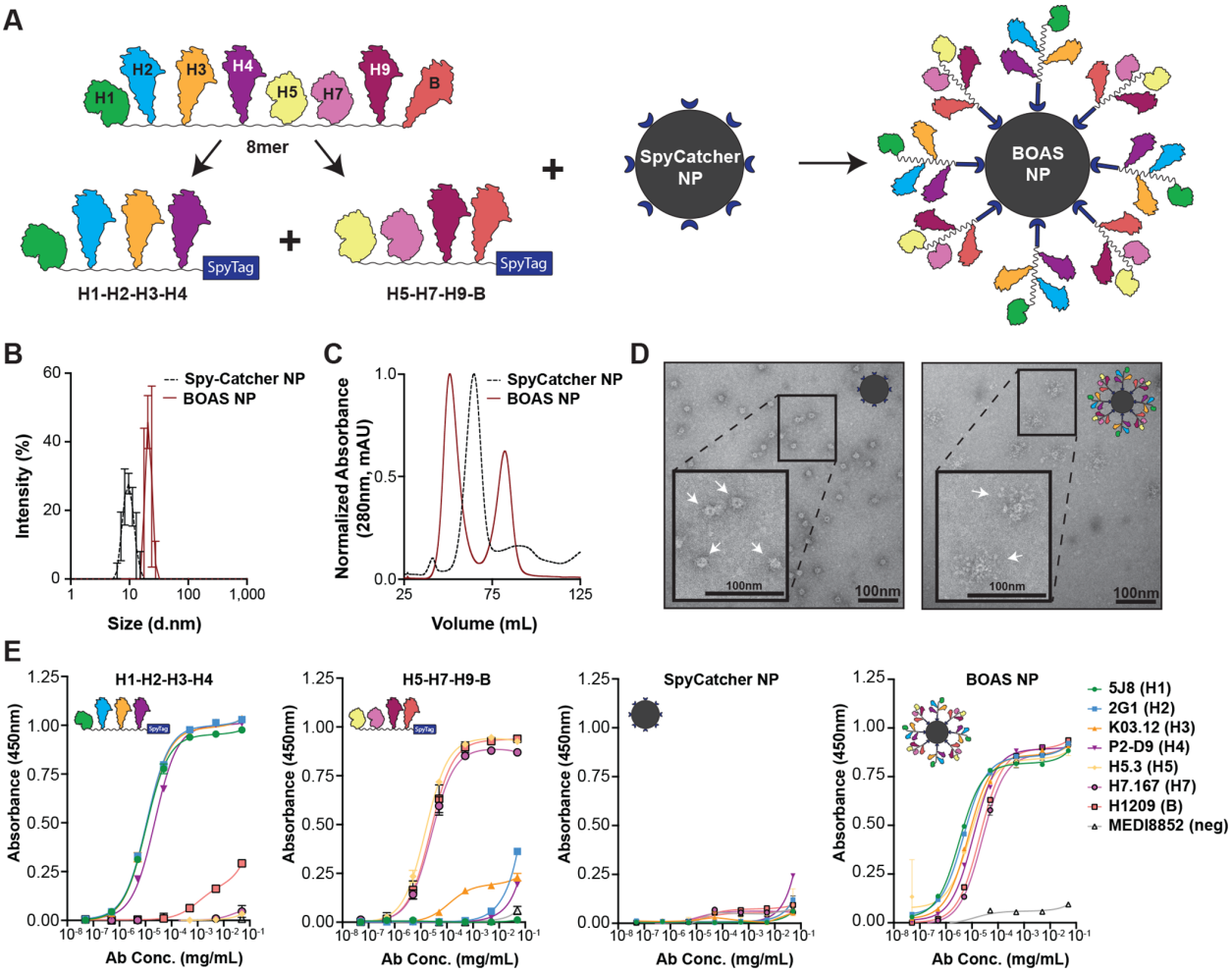

Figure 5: Design of BOAS nanoparticle (NP) immunogens- A) Schematic of design of BOAS nanoparticles. The eight original 8mer components were split into two 4mers, the first containing H1, H2, H3, and H4 (H1-H2-H3-H4), and the second containing H5, H7, H9, and B (H5-H7-H9-B). Each were expressed with an N-terminal SpyTag, then attached at equal molar ratios to an N-terminally fused SpyCatcher ferritin nanoparticle (SpyCatcher NP). This yields a ferritin nanoparticle with both 4mer BOAS conjugated to its surface (2x4mer BOAS NP). **B)** Dynamic light scattering (DLS) distributions of SpyCatcher NP and 2x4mer BOAS NP. Curves represent an average of 3 technical replicate measurements and error bars are +/- 1 s.d. **C)** Size exclusion traces of SpyCatcher NP and 2x4mer BOAS NP on an S400 column. **D)** Representative NS-EM image of SpyCatcher NP. Arrows indicate individual nanoparticles, and the inset is a 2X zoom of the boxed area. Representative NS-EM image of BOAS NP. Arrows indicate individual

758 nanoparticles, and the inset is a 2X zoom of the boxed area. **E)** ELISA of BOAS components,
759 SpyCatcher NP, and 2x4mer BOAS NP with structure-dependent subtype-specific antibodies and
760 a negative control stem-directed antibody, MEDI8852. Antibodies corresponding to each
761 component are as follows: 5J8 (RBS, H1), 2G1 (RBS, H2), K03.12 (RBS, H3), P2-D9 (H4), H5.3
762 (RBS, H5), H7.167 (RBS periphery, H7), H1209 (RBS, B).
763 ELISA data points are technical duplicates and error bars are +/- 1 s.d.

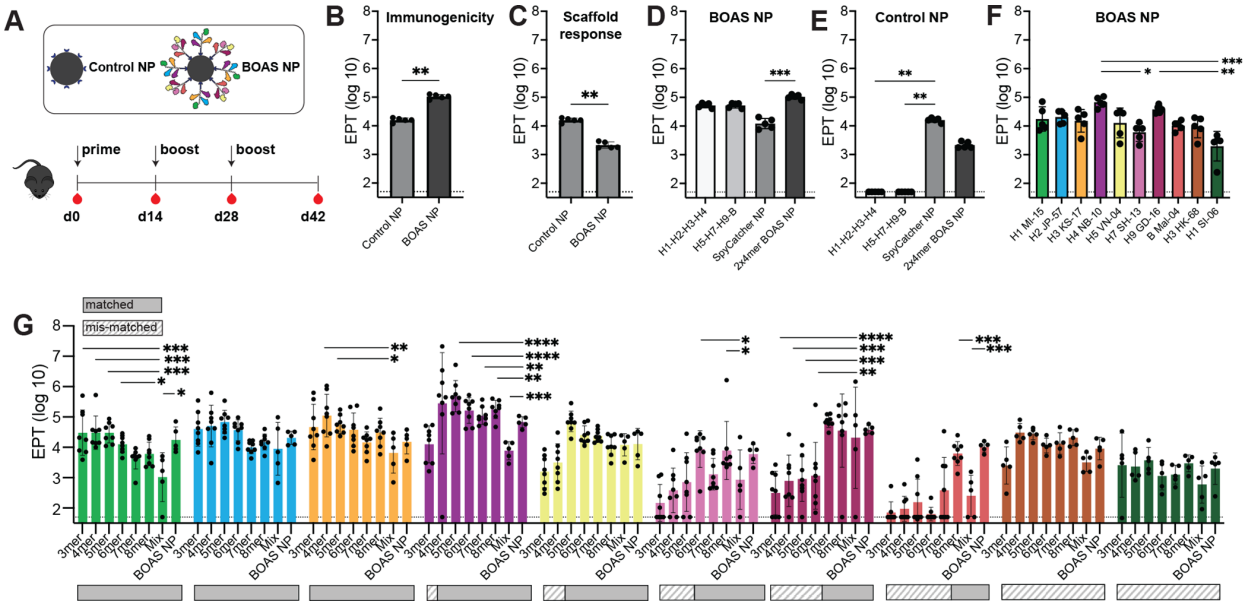

Figure 6: Murine Immunizations with BOAS NP A) Schematic of immunization regimen with 2x4mer BOAS NP and SpyCatcher NP control. Mice were primed with 20µg of NP, followed by two homologous boosts two weeks apart. **B)** Serum reactivity to each immunizing antigen at d42. ** p<0.01 as determined by Mann-Whitney test. **C)** Serum reactivity to Control NP scaffold by both groups. ** p<0.01 as determined by Mann-Whitney test. **D)** Serum reactivity elicited by BOAS NP group (n=5) at d42 to both individual BOAS components (H1-H2-H3-H4 and H5-H7-H9-B), Control NP, and BOAS NP. *** p < 0.001 as determined by Kruskal-Wallis test with Dunn's multiple comparison post hoc test. **E)** Serum reactivity elicited by Control NP group (n=5) at d42 to both individual BOAS components (H1-H2-H3-H4 and H5-H7-H9-B), Control NP, and BOAS NP. ** p < 0.01 as determined by Kruskal-Wallis test with Dunn's multiple comparison post hoc test. **F)** Serum reactivity elicited by BOAS NP group (n=5) to individual full-length HA components of BOAS at d42. * = p<0.05, ** = p<0.01, *** = p<0.001 as determined by Kruskal-Wallis test with Dunn's multiple comparison post hoc test. **G)** Serum reactivity to each matched and mis-matched individual full-length HA component of BOAS (H1/MI/15 light green, H2/JP/57 blue, H3/KS/17 light orange, H4/NB/10 purple, H5/VN/04 yellow, H7/SH/13 pink, H9/GD/16 maroon, B/Mal/04 salmon, H3/HK/68 dark orange, and H1/SI/06 dark green) by 3mer-8mer BOAS and BOAS NP. Solid bars below each plot indicate a matched sub-type, and striped bars indicate a mis-matched subtype (i.e. not present in the BOAS or NP). * = p<0.05, ** = p<0.01,

786 *** = $p<0.001$, **** = $p<0.0001$ as determined by Kruskal-Wallis test with multiple comparisons
787 relative to the mix control group. In all plots, data points for single time point antigen titers are
788 from individual mice (n=5 for BOAS NP and Mix cohorts, n=8 for 3mer-8mer BOAS studies),
789 bars represent mean titers and error bars are +/- 1 s.d.
790

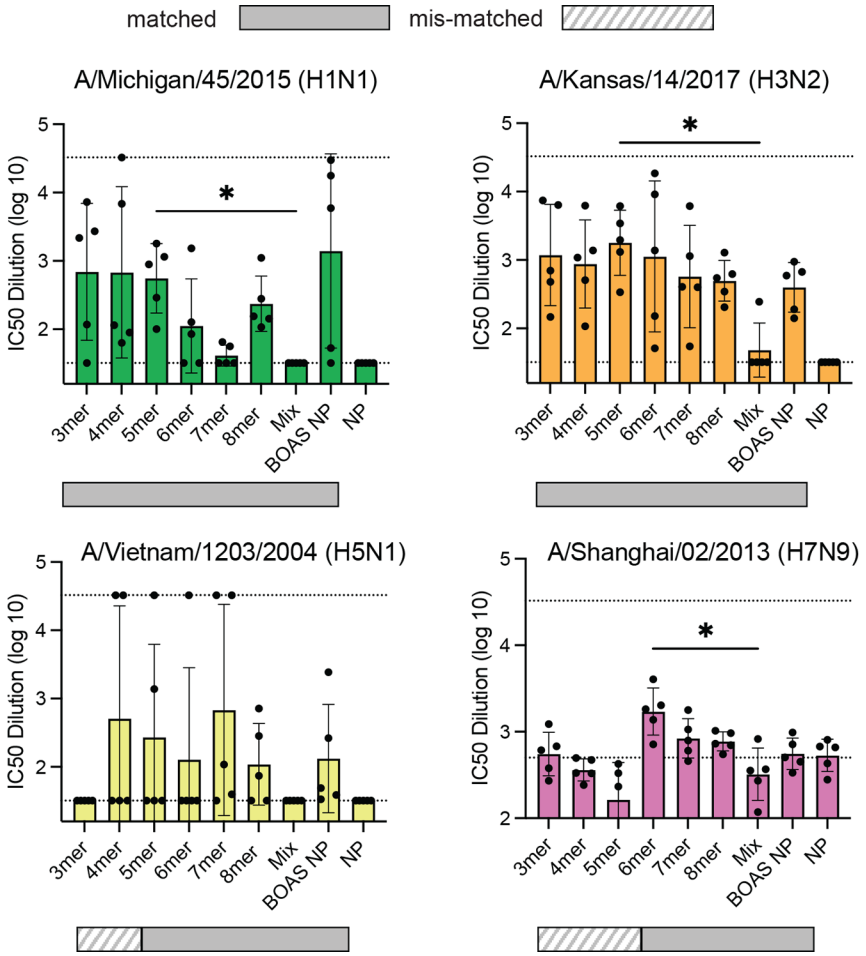

Figure 7: Microneutralization titers to matched and mis-matched virus- Microneutralization of matched and mis-matched psuedoviruses: H1N1 (green, top left), H3N2 (orange, top right), H5N1 (yellow, bottom left), and H7N9 viruses (pink, bottom right) with d42 serum. Solid bars below each plot indicate a matched sub-type, and striped bars indicate a mis-matched subtype (i.e. not present in the BOAS). NP negative controls were used to determine threshold for neutralization. Upper and lower dashed lines represent the first dilution (1:32) (for H1N1, H3N2, and H5N1) or neutralization average with negative control NP serum (H7N9), and the last serum dilution (1:32,768), respectively, and points at the dashed lines indicate IC50s at or outside the limit of detection. Individual points indicate IC50 values from individual mice from each cohort (n=5). The mean is denoted by a bar and error bars are +/- 1 s.d., * = $p<0.05$ as determined by a Kruskal-Wallis test with Dunn's multiple comparison post hoc test relative to the mix group.